View metadata, citation and similar papers at core.ac.uk

brought to you by CORE

provided by Elsevier - Publisher Connector

International Journal of Solids and Structures 45 (2008) 4543–4561

Contents lists available at ScienceDirect

International Journal of Solids and Structures

journal homepage: www.elsevier.com/locate/ijsolstr

Compression of solid and annular circular discs bonded to rigid surfaces

Seval Pinarbasi [a,*], Yalcin Mengi [b], Ugurhan Akyuz [c]

[a] Department of Civil Engineering, Kocaeli University, Veziroglu Campus, Izmit, 41040 Kocaeli, Turkey
[b] Department of Engineering Sciences, Middle East Technical University, 06531 Ankara, Turkey
[c] Department of Civil Engineering, Middle East Technical University, 06531 Ankara, Turkey

ARTICLE INFO

Article history:
Received 10 September 2007
Received in revised form 13 March 2008
Available online 4 April 2008

Keywords:
Compression
Bonded layer
Circular
Annular
Shape factor
Poisson's ratio
Radius ratio
Rubber
Elastomeric bearing
Seismic isolation

ABSTRACT

Although it is noted in the literature that the presence of a central hole in an elastic layer bonded to rigid surfaces can cause significant drop in its compression modulus, not much attention is given for investigating thoroughly and in detail the influence of the hole on the layer behavior. This paper presents analytical solutions to the problem of the uniform compression of bonded hollow circular elastic layers, which includes solid circular layers as a special case as the radius of hollow section vanishes. The closed-form expressions derived in this study are advanced in the sense that three of the commonly used assumptions in the analysis of bonded elastic layers are eliminated: (i) the incompressibility assumption, (ii) the "pressure" assumption and (iii) the assumption that plane sections remain plane after deformation. Through the use of the analytical solutions derived in the study, the compressive behavior of bonded circular discs is studied. Particular emphasis is given to the investigation of the effects of the existence of a central hole on the compression modulus, stress distributions and maximum stresses/strains in view of three key parameters: radius ratio of the hole, aspect ratio of the disc and Poisson's ratio of the disc material.

© 2008 Elsevier Ltd. All rights reserved.

1. Introduction

Proposed as an alternative approach to the traditional seismic resistant design strategies, seismic isolation technique has gained a practical importance when favorable engineering properties of "bonded" rubber layers are noticed. Composed of several thin rubber layers bonded to steel plates, steel-laminated rubber bearings are accepted as one of the most widely used isolation systems in seismic isolation approach. Although the use of bonded rubber layers for seismic protection of structures is relatively recent, their use in other engineering applications is not new. Rubber layers bonded to rigid surfaces have long been used as bridge bearings, elastic foundations to machinery and motors or as sealing components.

Thus, it is not surprising to see that the studies on bonded rubber layers, more generally on bonded elastic layers, go back as early as the beginning of the 20th century. According to Kelly (1997), "the first analysis of the compression stiffness was done using an energy approach by Rocard" in 1937 "and further developments were made by Gent and Lindley (1959) and Gent and Meinecke (1970)". These earliest studies put forward three basic assumptions for linear analysis of bonded elastic layers: (i) horizontal plane sections remain plane after deformation, (ii) initially vertical lateral surfaces take a parabolic shape in the deformed configuration and (iii) state of stress at any point in the material is dominated by the hydrostatic pressure. The method of formulations based on these assumptions is called the "pressure method" in the literature.

* Corresponding author. Tel.: +90 262 335 11 68; fax: +90 262 335 28 12.
E-mail address: sevalp@gmail.com (S. Pinarbasi).

0020-7683/$ - see front matter © 2008 Elsevier Ltd. All rights reserved.
doi:10.1016/j.ijsolstr.2008.03.026

In conjunction with the scope of the present paper, in what follows we review the earlier studies conducted to investigate the compressive behavior of bonded *circular* layers with or without a central circular hole, and for the studies involving other geometric shapes of bonded elastic layers, we refer to the extensive list of references presented in Pinarbasi et al. (2006).

Using a two-stage solution and assuming strict incompressibility (Poisson's ratio, $\nu = 0.5$), Gent and Lindley (1959) derived an expression for compression modulus of bonded circular discs. In their formulation, they used the above-mentioned three fundamental assumptions of the pressure method. Realizing the significant effect of material compressibility in "thin" rubber layers, Gent and Lindley (1959) also proposed an "ad hoc" modification to account for the bulk compressibility of rubber on compression modulus. Exact solutions to the compression problem of soft bonded elastic cylinders were obtained by Moghe and Neff (1971), who applied the exact boundary conditions at the traction-free faces. Involving infinite series of Bessel and trigonometric functions, their solutions, however, are not convenient for design calculations. Using a completely different approach, a dynamic relaxation method based on finite difference analysis, Holownia (1972) obtained stress distributions in circular rubber pads subject to uniform compression. However, their study was numerical and was valid only for limited values of aspect ratio and Poisson's ratio. Lindley (1979) may be accepted as the first researcher to derive a closed-form expression for compression modulus of "compressible" circular discs. In his analytical treatment, he assumed, besides the three fundamental assumptions of the pressure method, that the distribution of bulk strain over any horizontal section is parabolic. Using the fundamental assumptions of the pressure method but following a more direct procedure, Chalhoub and Kelly (1990) derived a closed-form expression for compression modulus of bonded circular discs. They emphasized the significance of including the compressibility effects in the analysis of "thin" rubber layers. In a similar way, using the displacement field proposed by Chalhoub and Kelly (1990) but removing the "pressure" assumption, Tsai and Lee (1998) derived a closed-form expression for compression modulus of bonded circular discs. Comparing their solution with the "pressure" solution, Tsai and Lee (1998) concluded that the pressure assumption is valid only for thin layers and nearly incompressible materials.

In earlier studies on bonded elastic layers, little attention has been given to annular discs. The study of Gent and Lindley (1959) may be accepted as one of the leading studies in that direction. In their experimental study, Gent and Lindley (1959) determined the compression modulus of bonded annular rubber blocks with different hole sizes. They concluded that the experimentally determined values for the compression modulus of the blocks with relatively large holes are "in good agreement with the relation predicted for infinitely long rectangular sectioned blocks" while those for the blocks with small holes "lie generally closer to the relation predicted for blocks of circular cross-section". It is interesting to note that although the experimental study of Gent and Lindley (1959) go back 1950s, it was in 1990s when the first analytical studies on bonded annular discs appeared in the literature (to the authors' best knowledge). This delay can be attributed to the fact that annular bonded layers started to attract the attention of researchers especially when the use of elastomeric bearings as seismic isolators became widespread in all over the world. It is now very well known that most of the seismic isolation elastomeric bearings are designed with a hole in their center. In a regular bearing, this hole is not too large usually since it is mainly used to prevent the dislocation of the reinforcing plates during the manufacturing process. On the other hand, it is almost impossible to design a relatively large bearing without a moderate-size hole in its center since, during the vulcanization process of such a bulky bearing, heat cannot penetrate into rubber thoroughly unless the bearing has additional free surfaces. It is also worth mentioning that the use of annular bearings may become advantageous in some particular applications of seismic isolation (e.g., isolation of a light-weight structure) (Kelly, 1997).

Realizing that the presence of even a very small hole in the center of a steel-laminated elastomeric bearing can decrease the compression modulus of the bearing enormously, Constantinou et al. (1992) analyzed the compression problem of annular bonded layers using the method of analysis proposed by Chalhoub and Kelly (1990). Based on their analytical study, Constantinou et al. (1992) concluded that the existence of a central hole does not only reduce the compression modulus of the bearing but also increase the shear strain developing in the elastomer due to compression. The study of Ling et al. (1995) differs from the study of Constantinou et al. (1992) mainly in the displacement field they used in their formulation. Their solutions were also based on incompressibility assumption. In an attempt to eliminate the "intuitive" assumptions used by Ling et al. (1995). Ling (1996) analyzed this "boundary layer problem" more rigorously; their solution, however, is valid for thin layers with slightly compressible materials.

The earlier studies on bonded elastic discs cited above have been focused mainly on the derivation of closed-form expressions for their compression modulus. However, as emphasized by Gent et al. (1974), the knowledge of detailed displacement/stress distributions and locations/magnitudes of critical local stresses in the layer is also essential for a rational design. Since most of the earlier studies on bonded elastic layers use the assumed displacement/stress fields, it is rather difficult to make a comprehensive and detailed study on the layer behavior using the solutions presented there. The approximate theory (Mengi, 1980) employed in the formulation proposed by Pinarbasi et al. (2006) may serve to this purpose. This theory is different from the others in that there is no need to start the formulation with some assumptions on stress and/or displacement distributions (other than those imposed by the order of the theory) or with some limitations on geometrical and/or material properties. In addition, since the effect of material compressibility is naturally included in the formulation, the solutions derived using this theory is valid not only for incompressible or nearly incompressible materials but also for highly compressible ones. Consequently, using the new formulation proposed by Pinarbasi et al. (2006), it is possible to derive advanced solutions which can be used for the detailed study of displacement/stress distributions in a bonded elastic layer.

At this point, it is important to note that even though the behavior of rubber is indeed highly nonlinear and it may undergo considerable finite deformations, in most of the previous analytical treatments, including the pressure method of analysis, rubber has been assumed to behave linearly and the derivations have been made for small strains because the use of finite strain analysis with nonlinear constitutive models leads to highly nonlinear and complex equations (Constantinou et al., 1992). It is also worth noting that a seismic isolation bearing is usually *not* allowed to carry large vertical loads since the horizontal stiffness of an elastomeric bearing decreases considerably with increasing vertical load (Naeim and Kelly, 1999), which may cause stability problems under large horizontal deformations. Kelly (1997) states the pressure levels at which isolation bearings are generally used as "5–7 MPa", which are well below the compression modulus of an elastomeric bearing unless its shape factor is very small. Thus, the simple predictions of linear theory may even be adequate for the analysis and design of most conventional seismic isolation bearings (Kelly, 1997).

The derivation of the formulation used in this study and its application to bonded elastic layers in the shape of "infinite" strips under three fundamental deformation modes (uniform compression, pure bending and apparent shear) were presented in Pinarbasi et al. (2006). In this paper, the application of this formulation to the compression problem of bonded circular discs with/without a central hole is presented. The study is organized as follows. First, as will be needed in the formulation, the field equations of the approximate theory are presented in cylindrical coordinates. Then, the approximate theory is applied to bonded elastic discs under uniform compression by keeping the order of the theory arbitrary and choosing the distribution functions employed in the theory as Legendre polynomials. The governing equations presented in general forms, in view of the displacement boundary conditions at the top and bottom faces of the layer, are then solved by using the first order theory for bonded elastic layers in the shape of solid and annular discs separately. Finally, using the analytical solutions, the compressive behavior of bonded hollow circular discs is studied in detail. Particular emphasis is given to the investigation of the effects of the presence of a central hole on the compression modulus, stress distributions and maximum stresses/strains in view of three key parameters: radius ratio of the hole (the ratio of the hole radius to the outer radius of the disc), aspect ratio of the disc (the ratio of the outer radius to the thickness) and Poisson's ratio of the elastic material.

2. Review of the approximate theory used in the study

Recently, a new analytical formulation was presented by Pinarbasi et al. (2006) to analyze linear behavior of elastic layers bonded to rigid surfaces, which has recently been extended to elastic layers bonded to flexible reinforcements (Pinarbasi and Mengi, 2008). In these studies, the formulation was presented in Cartesian coordinates to obtain general equations that can be applied to various shapes, such as, infinite-strip, square and rectangular shapes. For the application of the formulation to bonded circular discs (Fig. 1), it is convenient to present it in cylindrical coordinates (r,θ,z). In this section, first the approximate theory employed in the formulation, i.e., the theory due to Mengi (1980), is reviewed very shortly to introduce the notation used in the formulation and the equations of the theory in cylindrical coordinates are presented. Then, the theory is applied to the compression problem of rigidly bonded discs (Fig. 1) and the reduced governing equations are derived by keeping the order of the theory arbitrary.

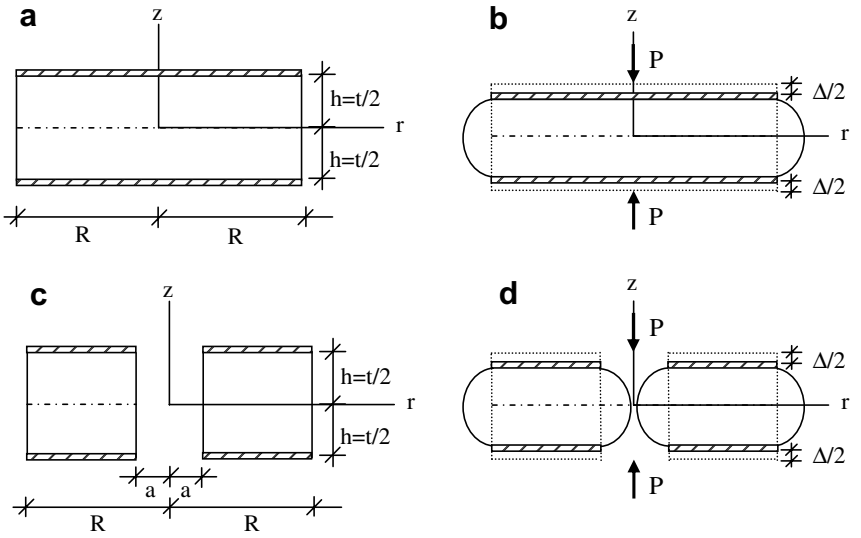

Fig. 1. Undeformed and deformed configurations for a bonded circular disc with and without a central hole under uniform compression.

2.1. Equations of the approximate theory in cylindrical coordinates

The approximate theory employed in the formulation, which was developed by Mengi (1980) using a modified version of the Galerkin method, assumes that the layer has a uniform thickness of $2h$, and that the layer material is isotropic and linearly elastic (Fig. 1a). A cylindrical coordinate system (r,θ,z) is defined with the origin at the center of the mid-plane (rz plane) of the layer such that z axis is perpendicular to the mid-plane as shown in Fig. 1a. The approximate theory contains two types of field variables: (i) "generalized variables" representing the *weighted* averages of displacements (u_i, $i = r,\theta,z$) and stresses (τ_{ij}, $i,j = r,\theta,z$) over the thickness of the layer; which are denoted, respectively, by u_i^n and τ_{ij}^n where $n = 0 - m$ for the mth order theory, and (ii) "face variables" representing the displacements and tractions on the lateral faces of the layer; denoted respectively by $u_i^{\pm} = u_i|_{z=\pm h}$ and $\tau_{zi}^{\pm} = \tau_{zi}|_{z=\pm h}$. The main difference of the theory due to Mengi (1980) over the others in the literature is the inclusion of face variables as field variables in this theory, which eliminates any inconsistency which may exist between displacement distributions assumed over the thickness of the layer and boundary conditions on its flat faces.

In the development of the theory, a set of distribution functions $\phi_n(\bar{z})(n = 0,1,2,\ldots;\bar{z} = z/h)$ is chosen. For mth order theory, the elements ϕ_n ($n = 0 - (m+2)$) are retained in the set. The theory is composed of two sets of equations. The first set contains the "weighted averages of elasticity equations", which are obtained by applying the operator $L^n = \frac{1}{2h}\int_{-h}^{+h}(.)\phi_n\,dz$ to these equations, where ϕ_n ($n = 0 - m$) are used as weighting functions. The second set is the "constitutive equations for face variables", which are obtained through the expansion of displacements in terms of the distribution functions as $u_i = \sum_{k=0}^{m+2} a_k^i \phi_k$, where a_k^i are some coefficients which depend on r and θ, and can be related to the field variables of the approximate theory (for details, see Pinarbasi et al. (2006)).

Following the procedure used in Pinarbasi et al. (2006), the governing equations of the approximate theory can be written in cylindrical coordinates as:

- weighted form of equilibrium equations ($n = 0 - m$):

$$\begin{aligned}
&\partial_r\tau_{rr}^n + \frac{1}{r}\partial_\theta\tau_{r\theta}^n + \frac{1}{r}(\tau_{rr}^n - \tau_{\theta\theta}^n) + (R_r^n - \bar{\tau}_{zr}^n) = 0\\
&\partial_r\tau_{r\theta}^n + \frac{1}{r}\partial_\theta\tau_{\theta\theta}^n + \frac{2}{r}\tau_{r\theta}^n + (R_\theta^n - \bar{\tau}_{z\theta}^n) = 0\\
&\partial_r\tau_{rz}^n + \frac{1}{r}\partial_\theta\tau_{\theta z}^n + \frac{1}{r}\tau_{rz}^n + (R_z^n - \bar{\tau}_{zz}^n) = 0
\end{aligned} \tag{1}$$

where

$$R_i^n = \frac{\hat{R}_i^n\phi_n(1)}{2h} \quad \text{where} \quad \hat{R}_i^n = \begin{cases} R_i^- = \tau_{zi}^+ - \tau_{zi}^- & \text{for even } n \\ R_i^+ = \tau_{zi}^+ + \tau_{zi}^- & \text{for odd } n \end{cases} \tag{2}$$

$$\tau_{ij}^n = L^n\tau_{ij}, \quad \bar{\tau}_{zi}^n = \bar{L}^n\tau_{zi} \quad \text{with} \quad \bar{L}^n = \frac{1}{2h}\int_{-h}^{h}(.)\frac{d\phi_n}{dz}\,dz \quad (i,j = r,\theta,z) \tag{3}$$

- weighted form of constitutive equations ($n = 0 - m$):

$$\begin{aligned}
\tau_{rr}^n &= \alpha\partial_r u_r^n + \lambda\left(\frac{1}{r}\partial_\theta u_\theta^n + \frac{1}{r}u_r^n\right) + \lambda(S_z^n - \bar{u}_z^n)\\
\tau_{\theta\theta}^n &= \alpha\left(\frac{1}{r}\partial_\theta u_\theta^n + \frac{1}{r}u_r^n\right) + \lambda(\partial_r u_r^n) + \lambda(S_z^n - \bar{u}_z^n)\\
\tau_{zz}^n &= \lambda\left(\partial_r u_r^n + \frac{1}{r}\partial_\theta u_\theta^n + \frac{1}{r}u_r^n\right) + \alpha(S_z^n - \bar{u}_z^n)\\
\tau_{r\theta}^n &= \mu\left(\frac{1}{r}\partial_\theta u_r^n + \partial_r u_\theta^n - \frac{1}{r}u_\theta^n\right), \quad \tau_{rz}^n = \mu\partial_r u_z^n + \mu(S_r^n - \bar{u}_r^n), \quad \tau_{\theta z}^n = \mu\frac{1}{r}\partial_\theta u_z^n + \mu(S_\theta^n - \bar{u}_\theta^n)
\end{aligned} \tag{4}$$

where

$$u_i^n = L^n u_i, \bar{u}_i^n = \bar{L}^n u_i, S_i^n = \frac{\hat{S}_i^n\phi_n(1)}{2h} \quad \text{where} \quad \hat{S}_i^n = \begin{cases} S_i^- = u_i^+ - u_i^- & \text{for even } n \\ S_i^+ = u_i^+ + u_i^- & \text{for odd } n \end{cases} \quad (i = r,\theta,z) \tag{5}$$

- constitutive equations for face variables:

$$\begin{aligned}
R_r^+ &= \mu(\partial_r S_z^+) + \frac{2\mu}{h}\left(\sum_{k=1,3}^{p'}\gamma_k u_r^k + \gamma^- S_r^-\right), \quad R_r^- = \mu(\partial_r S_z^-) + \frac{2\mu}{h}\left(\sum_{k=0,2}^{p}\gamma_k u_r^k + \gamma^+ S_r^+\right)\\
R_\theta^+ &= \mu\left(\frac{1}{r}\partial_\theta S_z^+\right) + \frac{2\mu}{h}\left(\sum_{k=1,3}^{p'}\gamma_k u_\theta^k + \gamma^- S_\theta^-\right), \quad R_\theta^- = \mu\left(\frac{1}{r}\partial_\theta S_z^-\right) + \frac{2\mu}{h}\left(\sum_{k=0,2}^{p}\gamma_k u_\theta^k + \gamma^+ S_\theta^+\right)
\end{aligned}$$

$$R_z^+ = \lambda\left(\partial_r S_r^+ + \frac{1}{r}\partial_\theta S_\theta^+ + \frac{1}{r}S_r^+\right) + \frac{2\alpha}{h}\left(\sum_{k=1,3}^{p'}\gamma_k u_z^k + \gamma^- S_z^-\right)$$
$$R_z^- = \lambda\left(\partial_r S_r^- + \frac{1}{r}\partial_\theta S_\theta^- + \frac{1}{r}S_r^-\right) + \frac{2\alpha}{h}\left(\sum_{k=0,2}^{p}\gamma_k u_z^k + \gamma^+ S_z^+\right) \tag{6}$$

In Eqs. (1)–(6), $\alpha = 2\mu + \lambda$, where λ and μ are Lamé's constants, ∂_i implies partial differentiation with respect to the related variable, and $p = m$ and $p' = m - 1$ for even m and $p = m - 1$ and $p' = m$ for odd m. It is worth mentioning that while deriving Eqs. (1)–(6), it is assumed that ϕ_n is even function of z for even n, and odd function of z for odd n. It may also be assumed without loss of generality that $\phi_n' = \frac{d\phi_n}{dz}$ is related to ϕ_j through some coefficients c_{nj} by $\phi_n' = \sum_{j=0}^{m} c_{nj}\phi_j$, implying that $\bar{\tau}_{zi}^n$ and $\bar{u}_i^n$ are related to τ_{zi}^n and u_i^n by

$$(\bar{\tau}_{zi}^n, \bar{u}_i^n) = \frac{1}{h}\sum_{j=0}^{m} c_{nj}(\tau_{zi}^j, u_i^j) \tag{7}$$

The constants γ_j, $\gamma^\pm$ and c_{nj} in Eqs. (6) and (7) can be determined whenever the distribution functions ϕ_n are chosen for any order of theory (refer to Mengi, 1980 and Pinarbasi et al., 2006 for more details).

Now, the re-emphasis of an important feature of the approximate theory, which is already mentioned, is in order. The approximate theory, as stated previously, contains generalized and face variables as field variables. The interaction between these two variables is described by the constitutive equations of face variables, i.e., by Eqs. (6). The appearance of the face variables as field variables facilitates and permits satisfying exactly the boundary conditions on the flat faces of the layer, e.g., on the bonded faces of the layer to be considered in the next section. Having determined the displacement face variables and generalized displacements through the solution of a problem (e.g., after solving the bonded layer problem considered in the next section), the displacement distributions in the layer may be evaluated from $u_i = \sum_{k=0}^{m+2} a_k^i \phi_k$ where a_k^i can be determined from Table 2 in terms of displacement face variables and generalized displacements; then, the substitution of these displacement distributions into the constitutive equations of linear elasticity yields the stress distributions in the layer.

2.2. Application of the formulation to the compression of bonded circular discs

Fig. 1a and c illustrate the undeformed configurations for a rigidly bonded circular disc of thickness t and radius R, respectively, in the absence and presence of a central circular hole with a radius a. When compressed by the amount Δ under a uniaxial compressive force P, the bonded discs have the deformed shapes illustrated in Fig. 1b and d. The object is to formulate and analyze each compression problem within the framework of the approximate theory reviewed in the previous section. In the analyses, the discs are referred to the same coordinate system employed in the theory. In the derivations and obtaining the results, the distribution functions in the approximate theory are chosen as Legendre polynomials of the first kind. The coefficients c_{nj}, a_k^i, γ_j and $\gamma^\pm$ of the theory for these distribution functions are listed in Tables 1 and 2 for various orders of theory.

It is obvious that, under uniform compression, regardless of the existence of a central hole, the deformation of the bonded disc is axisymmetric; $u_\theta = 0$, and radial and axial displacements are independent of θ; i.e., $u_r = u_r(r,z)$, $u_z = u_z(r,z)$. Furthermore, one can easily see that u_z is antisymmetric while u_r is symmetric about the mid-plane of the disc, which leads, in view of the special properties of the distribution functions, to

$$u_r^n = 0 \quad \text{and} \quad \bar{u}_z^n = 0 \quad \text{for odd } n, \qquad \bar{u}_r^n = 0 \quad \text{and} \quad u_z^n = 0 \quad \text{for even } n \tag{8}$$

The boundary conditions at the bonded faces of the disc implies

$$u_r^\pm = 0 \quad \text{and} \quad u_z^\pm = \mp\frac{\Delta}{2} \tag{9}$$

which leads to, in view of Eqs. (5),

$$S_r^\pm = S_z^+ = 0 \quad \text{and} \quad S_z^- = -\Delta \tag{10}$$
$$S_r^n = 0 \quad \text{for all } n, \qquad S_z^n = \begin{cases} -\Delta/t & \text{for even } n \\ 0 & \text{for odd } n \end{cases} \tag{11}$$

Table 1
c_{nj} coefficients (ϕ_n's are Legendre polynomials)

n	c_{nj} $(j = 0 - m)$
0	{0 0 0 0 0}
1	{1 0 0 0 0}
2	{0 3 0 0 0}
3	{1 0 5 0 0}
4	{0 3 0 7 0}

Table 2
Coefficients a_k^i and constants γ_j, $\gamma^{\pm}$ for the 0th, 1st and 2nd order theories (ϕ_n's are Legendre polynomials)

m	$a_k^i (k = 0 - (m+2))$	$\gamma_j (j = 0 - m)$	γ^+	γ^-
0	$\{u_i^0 \ S_i^-/2 \ S_i^+/2 - u_i^0\}$	$\{-3\}$	3/2	1/2
1	$\{u_i^0 \ 3u_i^1 S_i^+/2 - u_i^0 \ S_i^-/2 - 3u_i^1\}$	$\{-3 \ -15\}$	3/2	3
2	$\{u_i^0 \ 3u_i^1 \ 5u_i^2 S_i^-/2 - 3u_i^1 \ S_i^+/2 - 5u_i^2 - u_i^0\}$	$\{-10 \ -15 \ -35\}$	5	3

Then, Eqs. (4) and (6) reduce, in view of Eqs. (8)–(11), to the following uncoupled equations for the compression problems under consideration:

$$\left.\begin{aligned} \tau_{rr}^n &= \alpha\partial_r u_r^n + \tfrac{\lambda}{r} u_r^n - \tfrac{\lambda\Delta}{t} - \lambda\bar{u}_z^n \\ \tau_{\theta\theta}^n &= \lambda\partial_r u_r^n + \tfrac{\alpha}{r} u_r^n - \tfrac{\lambda\Delta}{t} - \lambda\bar{u}_z^n \\ \tau_{zz}^n &= \lambda\partial_r u_r^n + \tfrac{\lambda}{r} u_r^n - \tfrac{\alpha\Delta}{t} - \alpha\bar{u}_z^n \end{aligned}\right\} \quad \text{for even } n, \quad \tau_{rz}^n = \mu\partial_r u_z^n - \mu\bar{u}_r^n \quad \text{for odd } n \tag{12}$$

and

$$R_r^n = \frac{4\mu}{t^2}\left(\sum_{k=0,2}^{p} \gamma_k u_r^k\right) \quad \text{for even } n, \quad R_z^n = \frac{4\alpha}{t^2}\left(\sum_{k=1,3}^{p'} \gamma_k u_z^k - \Delta\gamma^-\right) \quad \text{for odd } n \tag{13}$$

where other R_i^n and τ_{ij}^n are zero. Through substitution of Eqs. (12) and (13) into Eqs. (1), one can obtain the following governing equations for the weighted displacements u_i^n:

$$\begin{aligned} &\alpha\partial_{rr} u_r^n + \frac{\alpha}{r}\partial_r u_r^n - \frac{\alpha}{r^2} u_r^n - \lambda\partial_r \bar{u}_z^n + \frac{4\mu}{t^2}\left(\sum_{k=0,2}^{p} \gamma_k u_r^k\right) = \bar{\tau}_{zr}^n \quad \text{for even } n \\ &\mu\partial_{rr} u_z^n + \frac{\mu}{r}\partial_r u_z^n - \mu\partial_r \bar{u}_r^n - \frac{\mu}{r}\bar{u}_r^n + \frac{4\alpha}{t^2}\left(\sum_{k=1,3}^{p'} \gamma_k u_z^k\right) - \frac{4\alpha}{t^2}\Delta\gamma^- = \bar{\tau}_{zz}^n \quad \text{for odd } n \end{aligned} \tag{14}$$

where, in view of Eq. (7),

$$(\bar{\tau}_{zi}^n, \bar{u}_i^n) = \frac{2}{t}\sum_{j=0}^{m} c_{nj}(\tau_{zi}^j, u_i^j) \tag{15}$$

in which τ_{zi}^j can be expressed in terms of u_i^n by Eqs. (12).

Eqs. (14) with Eqs. (12) and (15) constitute the reduced governing equations for the compression problem of bonded circular discs for any order of the theory. The presence of a central hole does *not* have any effect on these equations *but* influences the solutions through the boundary conditions. For the solutions of the differential equations in Eqs. (14), necessary boundary conditions are the stress-free boundary conditions at the lateral bulge-free surfaces, which can be written in terms of the weighted stress components τ_{ij}^n as

$$\tau_{rr}^n|_{r=r^*} = 0 \quad \text{for even } n, \quad \tau_{rz}^n|_{r=r^*} = 0 \quad \text{for odd } n \quad \text{where} \quad r^* = \begin{cases} R \text{ for solid sections} \\ a, R \text{ for hollow sections} \end{cases} \tag{16}$$

Additional conditions for the solid case come from the fact that displacements must be finite at the centroid of the disc, i.e., at $r = 0$.

Once Eqs. (14) are solved for u_i^n for any order of theory, determination of displacements, stress distributions or any other parameter, such as the compression modulus of the disc, is straightforward. Displacements can be determined using the relation $u_i = \sum_{k=0}^{m+2} a_k^i \phi_k$ with the values listed in Table 2 for a_i^k. Knowing the displacements, stress distributions can be derived from the stress–displacement relations of linear elasticity theory. For the determination of the compression modulus, the applied load P should be computed. Recalling that $R_z^- = 0$ for the compression problems under consideration, which implies that $\tau_{zz}^+ = \tau_{zz}^- = R_z^+/2$, P can be obtained from the integration of the axial face stress over the undeformed horizontal sectional area A of the disc:

$$P = -\int_A \tau_{zz}^{\pm} \, dA \quad \text{where} \quad \tau_{zz}^{\pm} = \frac{2\alpha}{t}\left(\sum_{k=1,3}^{p'} \gamma_k u_z^k\right) - \frac{2\alpha}{t}\gamma^- \Delta \tag{17}$$

The compression modulus E_c of a bonded circular disc, then, can be obtained from

$$E_c = \frac{P}{A\varepsilon_c} \quad \text{where} \quad \varepsilon_c = \frac{\Delta}{t} \quad \text{and} \quad A = \begin{cases} \pi R^2 & \text{for solid circular discs} \\ \pi(R^2 - a^2) & \text{for hollow circular discs} \end{cases} \tag{18}$$

3. Compression of bonded elastic circular discs

The equations presented in the previous section are derived for an arbitrary order of theory and can be solved for their unknowns once the order of the theory is specified. As shown in Pinarbasi et al. (2006), the 0th order theory (ZOT) indeed corresponds to averaging the field variables and equations of the linear theory of elasticity through the layer thickness, and therefore results in the same solutions based on "mean" pressure or "average" displacements with two kinematic assumptions: the parabolic bulging assumption and the assumption "plane sections remain plane after deformation" (e.g. Tsai and Lee, 1998). For this reason, in this study, only the derivations for the first order theory (FOT) are given.

3.1. Solid circular discs

When the compression problem for the bonded solid disc illustrated in Fig. 1a and b is formulated using FOT ($m = 1$, $p = 0$ and $p' = 1$), one has, in view of Eqs. (8), two unknown weighted displacements; u_r^0 and u_z^1, which can be determined by solving Eqs. (14) for both $n = 0$ and $n = 1$. For $n = 0$, the first of Eqs. (14) directly provides the governing equation for u_r^0. Using the relation given in Eq. (15) and the coefficients listed in Tables 1 and 2 for $m = 1$, this equation can be simplified as

$$\partial_{rr}u_r^0 + \frac{1}{r}\partial_r u_r^0 - \left(\frac{1}{r^2} + \beta_{r0}^2\right)u_r^0 = 0 \quad \text{where} \quad \beta_{r0}^2 = \frac{12\mu}{\alpha t^2} \tag{19}$$

the solution of which is

$$u_r^0 = a_{r0}I_1(\beta_{r0}r) + a_{r1}K_1(\beta_{r0}r) \tag{20}$$

where a_{r0} and a_{r1} are constants to be determined from the boundary conditions, and, I_1 and K_1 represent the modified Bessel functions of first and second kind of order one, respectively. As already mentioned, for a solid circular disc, u_r^0 must be finite at $r = 0$, which implies that a_{r1} is zero. The other integration constant, a_{r0}, can be obtained from the boundary condition $\tau_{rr}^0|_{r=R} = 0$, which in view of the first of Eqs. (12) with $n = 0$, requires

$$\left[\partial_r u_r^0 + \frac{\lambda}{\alpha}\frac{u_r^0}{r}\right]_{r=R} = \frac{\lambda\Delta}{\alpha t} \tag{21}$$

Then, the constants appearing in Eq. (20) would be

$$a_{r0} = \frac{\lambda\Delta}{\alpha t}\frac{1}{\beta_{r0}I_0(\beta_{r0}R) - \frac{2\mu}{\alpha R}I_1(\beta_{r0}R)} \quad \text{and} \quad a_{r1} = 0 \tag{22}$$

For $n = 1$, the equation comes from the weighted equilibrium equation in z direction, i.e., the second of Eqs. (14), which simplifies, in view of Table 2, as

$$\mu\partial_{rr}u_z^1 + \frac{\mu}{r}\partial_r u_z^1 - \mu\partial_r\bar{u}_r^1 - \frac{\mu}{r}\bar{u}_r^1 - \frac{60\alpha}{t^2}u_z^1 - \frac{12\alpha}{t^2}\Delta = \bar{\tau}_{zz}^1 \tag{23}$$

Considering the relation in Eq. (15) and using the third of Eqs. (12) with $n = 0$ for τ_{zz}^0, Eq. (23) can further be reduced, in view of Table 1, to

$$\partial_{rr}u_z^1 + \frac{1}{r}\partial_r u_z^1 - \beta_{z1}^2 u_z^1 = \frac{2}{t}\frac{\lambda+\mu}{\mu}\left[\partial_r u_r^0 + \frac{1}{r}u_r^0\right] + \frac{10\alpha\Delta}{\mu t^2} \quad \text{where} \quad \beta_{z1}^2 = \frac{60\alpha}{\mu t^2} \tag{24}$$

From the boundary condition at the lateral sides, one has, in view of the second of Eqs. (16) for $n = 1$, the condition $\tau_{rz}^1|_{r=R} = 0$, which implies

$$\left[\partial_r u_z^1\right]_{r=R} = \frac{2}{t}\left[u_r^0\right]_{r=R} \tag{25}$$

Finally, substitution of Eqs. (20) and (22) into Eqs. (24) and (25) leads to the following governing equation and boundary condition for u_z^1:

$$\partial_{rr}u_z^1 + \frac{1}{r}\partial_r u_z^1 - \beta_{z1}^2 u_z^1 = \frac{2}{t}\frac{\lambda+\mu}{\mu}\left[a_{r0}\beta_{r0}I_0(\beta_{r0}r)\right] + \frac{10\alpha\Delta}{\mu t^2} \tag{26}$$

with

$$\left[\partial_r u_z^1\right]_{r=R} = \frac{2a_{r0}}{t}I_1(\beta_{r0}R) \tag{27}$$

The solution of Eq. (26) is, subject to the boundary condition in Eq. (27) with the condition that u_z^1 must be finite at $r = 0$,

$$u_z^1 = a_{z1}I_0(\beta_{z1}r) + \frac{2}{t}\frac{\mu+\lambda}{\mu}\frac{\beta_{r0}}{\beta_{r0}^2 - \beta_{z1}^2}a_{r0}I_0(\beta_{r0}r) - \frac{\Delta}{6} \tag{28}$$

where

$$a_{z1} = \frac{2a_{r0}}{t}\frac{I_1(\beta_{r0}R)}{\beta_{z1}I_1(\beta_{z1}R)}\left[1 - \frac{\mu+\lambda}{\mu}\frac{\beta_{r0}^2}{\beta_{r0}^2-\beta_{z1}^2}\right] \tag{29}$$

Consequently, u_r and u_z can be determined for the solid circular case as

$$\begin{aligned} u_r &= \frac{3}{2}a_{r0}I_1(\beta_{r0}r)\left(1-\frac{4z^2}{t^2}\right) \\ u_z &= \frac{30}{t}a_{r0}\left\{\begin{array}{l}\frac{I_1(\beta_{r0}R)I_0(\beta_{z1}r)}{\beta_{z1}I_1(\beta_{z1}R)}\left[1-\frac{\mu+\lambda}{\mu}\frac{\beta_{r0}^2}{\beta_{r0}^2-\beta_{z1}^2}\right] \\ +I_0(\beta_{r0}r)\frac{\mu+\lambda}{\mu}\frac{\beta_{r0}}{\beta_{r0}^2-\beta_{z1}^2}\end{array}\right\}\left(\frac{z}{t}\right)\left(1-\frac{4z^2}{t^2}\right)-\Delta\frac{z}{t} \end{aligned} \tag{30}$$

From Eqs. (17) and (18), one can also obtain the effective compression modulus E_c as:

$$E_c = \alpha - \frac{\lambda^2}{\alpha(\beta_{r0}R)\frac{I_0(\beta_{r0}R)}{2I_1(\beta_{r0}R)}-\mu} \tag{31}$$

It is to be noted that FOT leads to the same E_c expression derived by Tsai and Lee (1998). Also, it can be verified that this expression is the same as that predicted by ZOT for E_c. This is also the case for u_r. Thus, similar to the infinite-strip case studied by Pinarbasi et al. (2006), the main contribution of the use of FOT in the formulation is the elimination of the commonly used assumption that horizontal plane sections remain plane and horizontal during deformation. Removal of this assumption leads to an improved expression for the axial displacement u_z, which, in turn, improves the stress expressions and permits the study of the stress distributions over any section of the disc thoroughly.

Here, it is valuable to compare the stress distributions between ZOT and FOT. Fig. 2 shows radial stress distributions in a low-shape-factored (LSF) layer ($S = 0.75$) and a high-shape-factored (HSF) layer ($S = 30$) for various Poisson's ratios.

As shown in the figure, although ZOT can satisfactorily predict the behavior of an HSF layer even when the layer is highly compressible ($\nu = 0.3$), it cannot predict the nonuniform stress distribution over the layer thickness for the LSF layer, which requires the elimination of the "plane sections remain plane" assumption.

3.2. Hollow circular discs

As already mentioned, the solution of annular discs differs from the solution of solid discs only in the boundary conditions. That is, the governing equations derived for solid circular sections using FOT, i.e., Eqs. (19) and (24), are valid also for hollow circular sections; but, in this case, instead of vanishing weighted displacements at the centroid, one has, in view of Eqs. (16), the following two boundary conditions in addition to those in Eqs. (21) and (25):

$$\left[\partial_r u_r^0 + \frac{\lambda}{\alpha}\frac{u_r^0}{r}\right]_{r=a} = \frac{\lambda\Delta}{\alpha t} \quad \text{and} \quad \left[\partial_r u_z^1\right]_{r=a} = \frac{2}{t}\left[u_r^0\right]_{r=a} \tag{32}$$

From the boundary conditions given in Eq. (21) and the first of Eqs. (32), the integration constants a_{r0} and a_{r1} appearing in Eq. (20) can be determined as

$$a_{r0} = \frac{\lambda\Delta}{t}\frac{A_4 - A_2}{A_1A_4 - A_2A_3} \quad \text{and} \quad a_{r1} = \frac{\lambda\Delta}{t}\frac{A_3 - A_1}{A_1A_4 - A_2A_3} \tag{33}$$

where

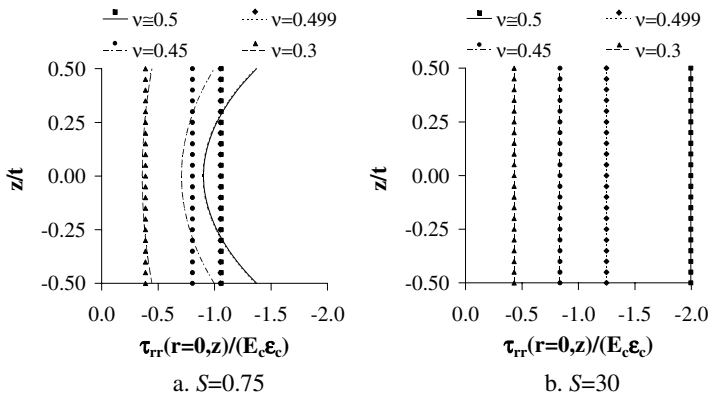

Fig. 2. Comparison of the predictions of ZOT (discrete points) and FOT (continuous lines) for radial stress distribution in bonded solid circular discs with different geometrical and material properties.

$$A_1 = \alpha\beta_{r0}I_0(\beta_{r0}R) - 2\mu\frac{I_1(\beta_{r0}R)}{R}, \quad A_2 = \alpha\beta_{r0}K_0(\beta_{r0}R) + 2\mu\frac{K_1(\beta_{r0}R)}{R}$$
$$A_3 = \alpha\beta_{r0}I_0(\beta_{r0}a) - 2\mu\frac{I_1(\beta_{r0}a)}{a}, \quad A_4 = \alpha\beta_{r0}K_0(\beta_{r0}a) + 2\mu\frac{K_1(\beta_{r0}a)}{a} \tag{34}$$

Substitution of Eqs. (20) with Eqs. (33) into Eqs. (24) and (25) and the second of Eqs. (32) gives the following governing equation and boundary conditions for u_z^1:

$$\partial_{rr}u_z^1 + \frac{1}{r}\partial_r u_z^1 - \beta_{z1}^2 u_z^1 = \frac{2}{t}\frac{\lambda+\mu}{\mu}[a_{r0}\beta_{r0}I_0(\beta_{r0}r) - a_{r1}\beta_{r0}K_0(\beta_{r0}r)] + \frac{10\alpha\Delta}{\mu t^2} \tag{35}$$

with

$$[\partial_r u_z^1]_{r=R} = \frac{2}{t}[a_{r0}I_1(\beta_{r0}R) + a_{r1}K_1(\beta_{r0}R)], \quad [\partial_r u_z^1]_{r=a} = \frac{2}{t}[a_{r0}I_1(\beta_{r0}a) + a_{r1}K_1(\beta_{r0}a)] \tag{36}$$

Solving Eq. (35) with the conditions given in Eqs. (36), one can obtain u_z^1 as

$$u_z^1 = a_{z1}I_0(\beta_{z1}r) + a_{z2}K_0(\beta_{z1}r) + B[a_{r0}I_0(\beta_{r0}r) - a_{r1}K_0(\beta_{r0}r)] - \frac{\Delta}{6} \tag{37}$$

where

$$B = \frac{2}{t}\frac{\mu+\lambda}{\mu}\frac{\beta_{r0}}{\beta_{r0}^2 - \beta_{z1}^2} \tag{38}$$

$$a_{z1} = \frac{C_1K_1(\beta_{z1}a) - C_2K_1(\beta_{z1}R)}{\beta_{z1}[I_1(\beta_{z1}R)K_1(\beta_{z1}a) - I_1(\beta_{z1}a)K_1(\beta_{z1}R)]}$$
$$a_{z2} = \frac{C_1I_1(\beta_{z1}a) - C_2I_1(\beta_{z1}R)}{\beta_{z1}[I_1(\beta_{z1}R)K_1(\beta_{z1}a) - I_1(\beta_{z1}a)K_1(\beta_{z1}R)]} \tag{39}$$

with

$$C_1 = [a_{r0}I_1(\beta_{r0}R) + a_{r1}K_1(\beta_{r0}R)] \times \left[\frac{2}{t} - B\beta_{r0}\right]$$
$$C_2 = [a_{r0}I_1(\beta_{r0}a) + a_{r1}K_1(\beta_{r0}a)] \times \left[\frac{2}{t} - B\beta_{r0}\right] \tag{40}$$

Then, one has the following expressions for u_r and u_z for a bonded annular layer:

$$u_r = \frac{3}{2}[a_{r0}I_1(\beta_{r0}r) + a_{r1}K_1(\beta_{r0}r)]\left(1 - \frac{4z^2}{t^2}\right)$$
$$u_z = 15\left\{\begin{array}{l} a_{z1}I_0(\beta_{z1}r) + a_{z2}K_0(\beta_{z1}r) \\ +B[a_{r0}I_0(\beta_{r0}r) - a_{r1}K_0(\beta_{r0}r)] \end{array}\right\}\left(\frac{z}{t}\right)\left(1 - \frac{4z^2}{t^2}\right) - \Delta\frac{z}{t} \tag{41}$$

Substituting the expression for u_z^1 in Eq. (17) and then using Eq. (18), E_c can be obtained as

$$E_c = \alpha - \frac{2\lambda}{\frac{\Delta}{t}(R^2 - a^2)}\{a_{r0}[RI_1(\beta_{r0}R) - aI_1(\beta_{r0}a)] - a_{r1}[RK_1(\beta_{r0}R) - aK_1(\beta_{r0}a)]\} \tag{42}$$

It can be shown that the above expressions for u_r and E_c are identical to those predicted by ZOT. To our best knowledge, there are no such solutions, i.e., solutions based on "mean" pressure or "average" displacements with two kinematic assumptions, in the literature for compressive behavior of bonded annular discs. Thus, as far as the compressive behavior of bonded hollow circular discs is concerned, not only the expression in the second of Eqs. (41) but also the expressions in the first of

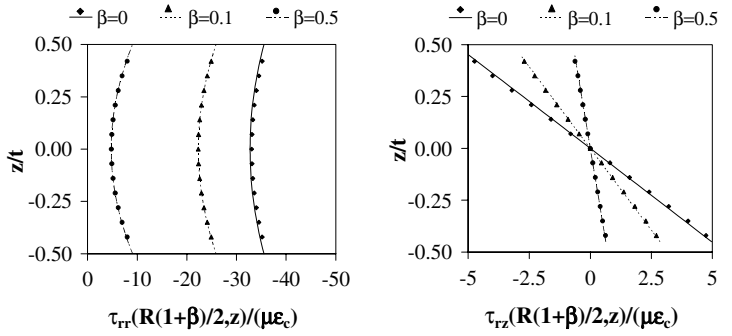

Fig. 3. Comparison of FOT (continuous lines) and BEM (discrete points) predictions for radial and shear stress distributions through the layer thickness in a bonded annular disc ($R/t = 4$, $\nu = 0.499$) with different radius ratios.

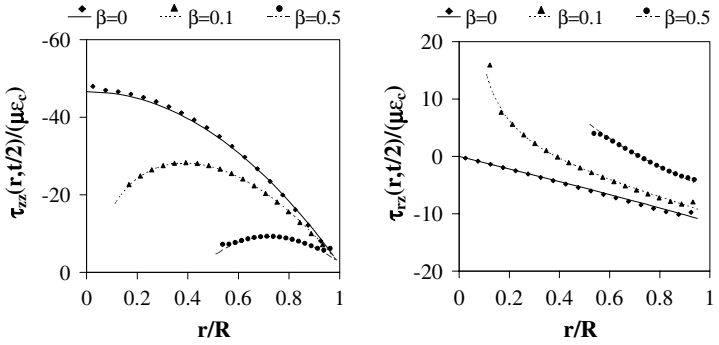

Fig. 4. Comparison of FOT (continuous lines) and BEM (discrete points) predictions for axial and shear stress distributions over the bonded faces in a bonded annular disc ($R/t = 4$, $\nu = 0.499$) with different radius ratios.

Eqs. (41) and (42) represent advanced solutions, which are presented first time, to our best knowledge, in the present study. Similar to the solid circular case, the expression in the second of Eqs. (41) further eliminates the commonly used assumption in the literature: horizontal plane of the layer remains plane and horizontal during deformation, and permits studying the stress distributions in hollow circular discs correctly.

FOT solutions for bonded annular discs are verified with the numerical results obtained using boundary element method (BEM) for an LSF layer ($R/t = 4$) with two different hole diameters; $a/t = 0.4$ and 2, corresponding to the radius ratios $\beta = R/a = 0.1$ and 0.5, respectively (see Figs. 3 and 4). The predictions for the solid circular layer (i.e., $\beta = 0$) are also included in the plots so that the expressions derived for the solid case can also be assessed. A relatively high value of Poisson's ratio, $\nu = 0.499$, is selected in this numerical problem to simulate the problem of a bonded *rubber* layer. BEM analysis is performed using the FORTRAN program developed by Ozkan (1995) for the elastodynamic analysis of axisymmetric bodies. As seen from Figs. 3 and 4, stress predictions of FOT are very close to the BEM results for all studied models.

4. Discussions of analytical solutions

Considering that there is rather limited work in the literature on bonded annular layers, the discussion that is presented in the following sections focuses on bonded hollow circular discs (HC-discs). Since the solutions for HC-discs contain those of solid circular discs (C-discs) as a special case, these discussions inherently include also C-discs.

From Eqs. (41) and (42), it may be noticed that the compressive behavior of a bonded HC-disc of outer radius R, inner radius a and thickness t, is controlled by three main parameters: (i) the size of the centrally placed hole, (ii) compressibility of the elastic material and (iii) aspect ratio of the disc. Surely, the radius ratio for the hole $\beta = a/R$ is the first key parameter for an annular disc.

As for the second parameter, i.e., the compressibility of elastic material, earlier studies on bonded elastic layers (e.g., Gent and Lindley, 1959; Kelly, 1997) have already shown that the effects of the bonded surfaces on compressive behavior of a bonded elastic layer highly depend not only on the geometric but also on the material properties of the layer, and become much more pronounced as the material compressibility decreases, i.e., as Poisson's ratio approaches 0.5. Lindley (1968) explains this dependence with the statement that "for materials such as rubber which have a low shear modulus but a relatively high bulk modulus, any restrictions on their freedom to change shape can have a very marked effect on their stiffness in compression". Earlier studies (e.g., Tsai and Lee, 1998; Pinarbasi et al., 2006) have also pointed out that the incompressibility assumption (i.e., assuming $\nu = 0.5$) is, in general, not valid for bonded *rubber* layers since the behavior of a bonded elastic layer with, for example, $\nu = 0.499$, which seems to be very close to 0.5, may considerably be different than its incompressible behavior. It is now well known that the compressibility of rubber is mainly related to its composition. As an example, while ν is 0.49989 for natural gum rubber, it can be as low as 0.39 for foam rubber (Lindley, 1968). Thus, considering the significance of material compressibility on compressive behavior of bonded elastic layers, Poisson's ratio of the elastic material ν is taken as the second key parameter in this study.

Incorporation of the third parameter; i.e., aspect ratio of the layer, into the numerical study of bonded annular discs, however, is not as straightforward as in the other shapes. Unlike a C-disc, for which the shape factor (the ratio of one bonded area to its bulge-free area) is $S = R/2t$, it is not possible to relate the shape factor of an HC-disc, which is $S = S_0(1-\beta)$ with $S_0 = R/2t$, directly to its aspect ratio. It can be seen that S_0, called "initial shape factor" (Ling et al., 1995), simply equals to the shape factor of the corresponding C-disc with the same external radius and thickness. In view of the discussions presented above, in this section, besides $\{\beta,\nu\}$,S_0 (instead of the shape factor S) is preferred to be taken as the third key parameter controlling the compressive behavior of bonded HC-discs.

4.1. Compression modulus

The graphs in Fig. 5a illustrate the effect of radius ratio on compression modulus of a bonded HC-disc, denoted as $E_{c,HC}$, for two specific values of initial shape factor; $S_0 = 2$, representing LSF discs and $S_0 = 30$, representing HSF discs. To study the

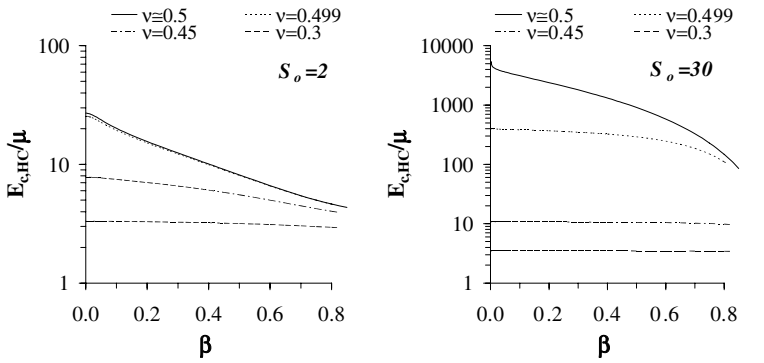

a. $E_{c,HC}$, normalized with respect to μ

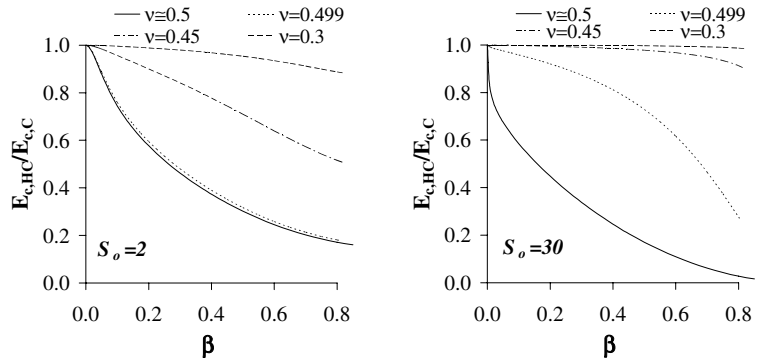

b. $E_{c,HC}$, normalized with respect to $E_{c,C}$

Fig. 5. Effect of radius ratio on $E_{c,HC}$, normalized with respect to (a) μ and (b) $E_{c,C}$, for two different initial shape factors $S_0 = 2,30$.

behavior of the discs over a wide range of compressibility, the variations are plotted for four different levels of material compressibility; $\nu \cong 0.5$, 0.499, 0.45, 0.3. From Fig. 5a, it is seen that the compression modulus of a bonded circular disc with a central hole can be much smaller than that of a solid disc. However, since the $E_{c,HC}$ values change considerably with S_0, it seems to be logical to replot these graphs by using a different normalization.

The graphs presented in Fig. 5b are plotted by normalizing $E_{c,HC}$ by that of the corresponding C-disc with the same aspect ratio and material properties, denoted as $E_{c,C}$. As seen from the plots, reduction in $E_{c,HC}$ with increasing β is drastic especially if ν is close to 0.5. This is mainly due to the fact that the presence of even a very small hole in the center of the layer modifies the axial stress distribution over the cross-section enormously. It is important to note that the decrease in $E_{c,HC}$ with increasing β is *not* linear in general. For incompressible case, while a "jump-like" decrease is observed at very small values of β for $S_0 = 30$, a somewhat more gradual decrease is seen for $S_0 = 2$. The behavior of the HSF disc ($S_0 = 30$) is different from that of the LSF disc ($S_0 = 2$) also in that while the LSF disc is not affected from the existence of slight compressibility ($\nu = 0.499$) in the disc material, the HSF disc is influenced considerably. It is striking to see that, for $S_0 = 30$ and $\beta = 0.1$, the reduction in compression modulus is more than 40% for $\nu \cong 0.5$ while it is less than 13% for $\nu = 0.499$. Fig. 5 shows further that, for a highly compressible materials ($\nu = 0.3$), the compression modulus of an HC-disc is almost independent from the radius ratio of the hole unless the hole is too large, implying that $E_{c,HC} = E_{c,C}$ for highly compressible materials. We think that the difference between the behaviors of LSF and HSF layers in Fig. 5 is due to the sensitivity of the distributions of the normal stress τ_{zz} over horizontal sections of the layers to the shape factor $S = S_0(1 - \beta)$ and Poisson's ratio ν, in particular, when S_0 is large and ν is close to 0.5.

The graphs in Fig. 6 show the variation of compression modulus with Poisson's ratio for two specific β values, 0.01 and 0.1, and four different S_0 values, 2, 5, 15 and 30. The predictions of the pressure method (PM) are also included, in discrete points, in the graphs so that PM can also be assessed. As already mentioned, PM solutions for annular discs were derived by Constantinou et al. (1992). From Fig. 6, it is seen that for all studied values of S_0 and β,E_c increases with increasing ν until the asymptotic incompressible value is attained. LSF layers attain their limiting incompressible behavior at much smaller values of ν, which is why they are *not* influenced from the existence of slight compressibility ($\nu = 0.499$). On the other hand, the moduli of slightly compressible HSF discs are considerably different from their incompressible moduli even for $\beta = 0.01$. Fig. 6 also shows that PM predictions are accurate only if S_0 is large and ν is close to 0.5. While FOT satisfactorily converges to the limiting value of $E/\mu = 2.0$ as ν approaches to zero, PM predictions drop even below this value.

FOT predictions are also compared with the solutions derived by Ling (1996). Fig. 7 shows such a comparison for incompressible materials and for various geometric properties. The agreement in the figure is mainly due to the fact that both the

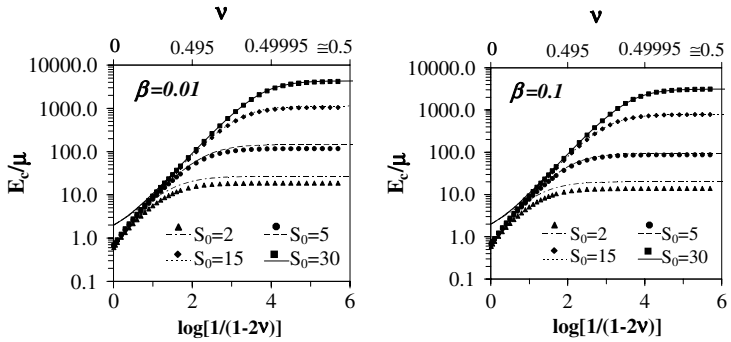

Fig. 6. Comparison of FOT (continuous lines) and PM (discrete points) predictions for compression modulus of bonded annular discs with different geometrical and material properties.

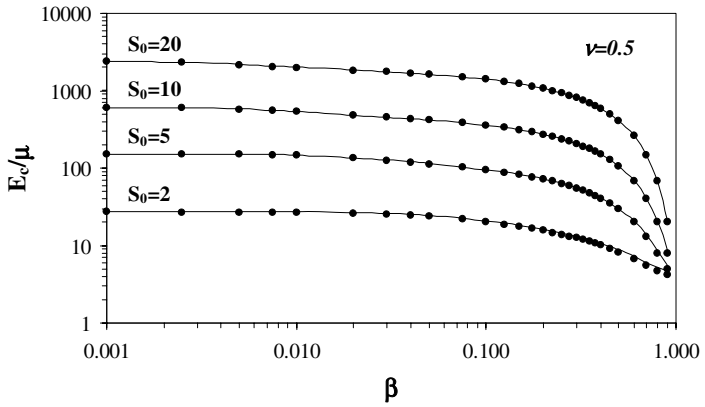

Fig. 7. Comparison of the FOT predictions (continuous lines) with the predictions of Ling (1996) (discrete points) for compression modulus of bonded annular discs with various geometrical properties.

"pressure" and "plane sections remain plane" assumptions are removed in the formulations of these two theories. However, it is to be noted that the closed-form expressions of Ling (1996) are given only for strictly incompressible materials, no such expressions are presented in that work for compressible case.

4.2. Stress distributions

The graphs presented in Figs. 8 and 9 illustrate the effect of radius ratio on axial (τ_{zz}) and shear (τ_{rz}) stress distributions in radial direction over their most critical sections (i.e., τ_{zz} at $z = 0$, τ_{rz} at $z = \pm t/2$) in a bonded annular disc under uniform compression for two different values of initial shape factor and four different values of β; 0, 0.01, 0.1 and 0.5. The value of $\beta = 0$, implying a solid section, is included for comparison. In the graphs, stress values are normalized by $E_c\varepsilon_c$.

From Fig. 8a and b, it can be seen that while the axial stress distribution in the LSF disc is *not* influenced from the existence of a very small hole ($\beta = 0.01$) significantly, the presence of even such a small hole can cause drastic change in the axial stress distribution in the HSF disc. The main effect of the hole is to shift the location of the maximum stress toward the center of the "ring" (i.e., $r = R(1 + \beta)/2$) and to decrease the stress values near the hole noticeably. As expected, such a modification in axial stress distribution also decreases the magnitude of maximum axial stress $(\tau_{zz})_{max}$ considerably if the layer material is incompressible. What is less expected is perhaps that, the value of $(\tau_{zz})_{max}$ in the HSF disc does not change significantly if the material has even slight compressibility ($\nu = 0.499$). In fact, for compressible and highly compressible materials ($\nu \leqslant 0.45$), it can even be concluded that the presence of a central hole in a bonded circular disc does not affect the axial stress distribution, neither its shape nor its peak value, significantly unless S_0 is too small and/or β is too large. Although the axial stress distribution in the LSF layer seems to be insensitive to the presence of a very small hole in its center, it starts to "sense" the existence of the hole when β is "sufficiently" large (first of Fig. 8c). Fig. 8 also shows that the shape of the axial stress distribution in a bonded circular disc, which is symmetric about the center of the disc when it is solid (Fig. 8a), changes with increasing β in such a way that for a sufficiently large value of β, the stress distribution becomes, again, symmetric, but now, about the center of the "ring" (Fig. 8d).

In contrast to the normal stresses, which decrease noticeably near $r = \beta R$, shear stress in a bonded annular layer increases with increasing β, as shown in Fig. 9. Shear stress near the hole is in general larger than that near the other surface (Fig. 9c).

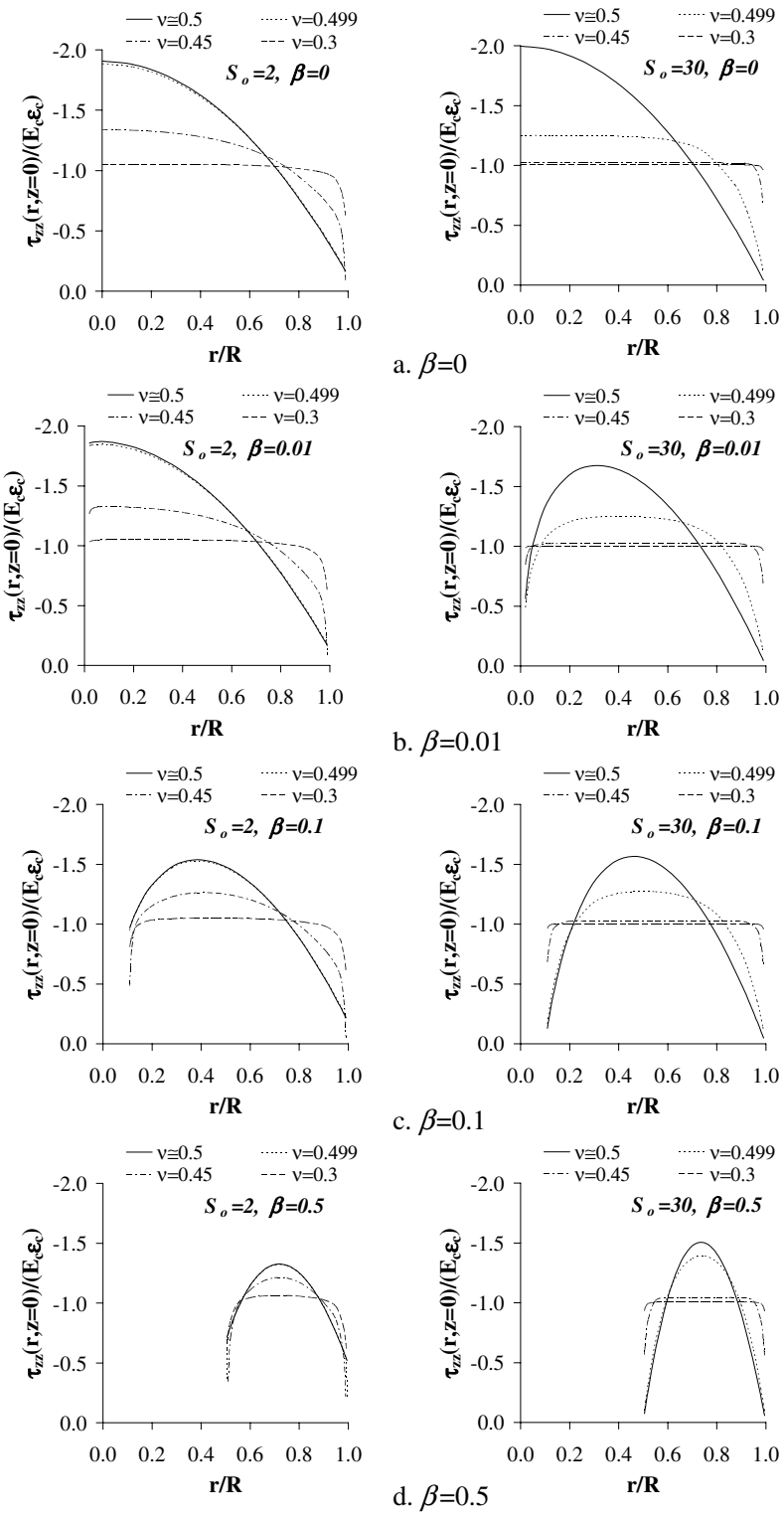

Fig. 8. Effect of radius ratio on axial stress distribution in radial direction in bonded annular layers with $S_0 = 2$ and $S_0 = 30$.

In the limit, when the layer starts to behave as if it were an infinite-strip (IS) layer, they become equal. Here, it is to be noted that the shear stresses at the edges of the bonded faces are nonzero, which is due to the singular nature of the edge points. The singularities at these points stem from no-slip conditions on bonded faces; in fact, as noted by Papoulia and Kelly (1996),

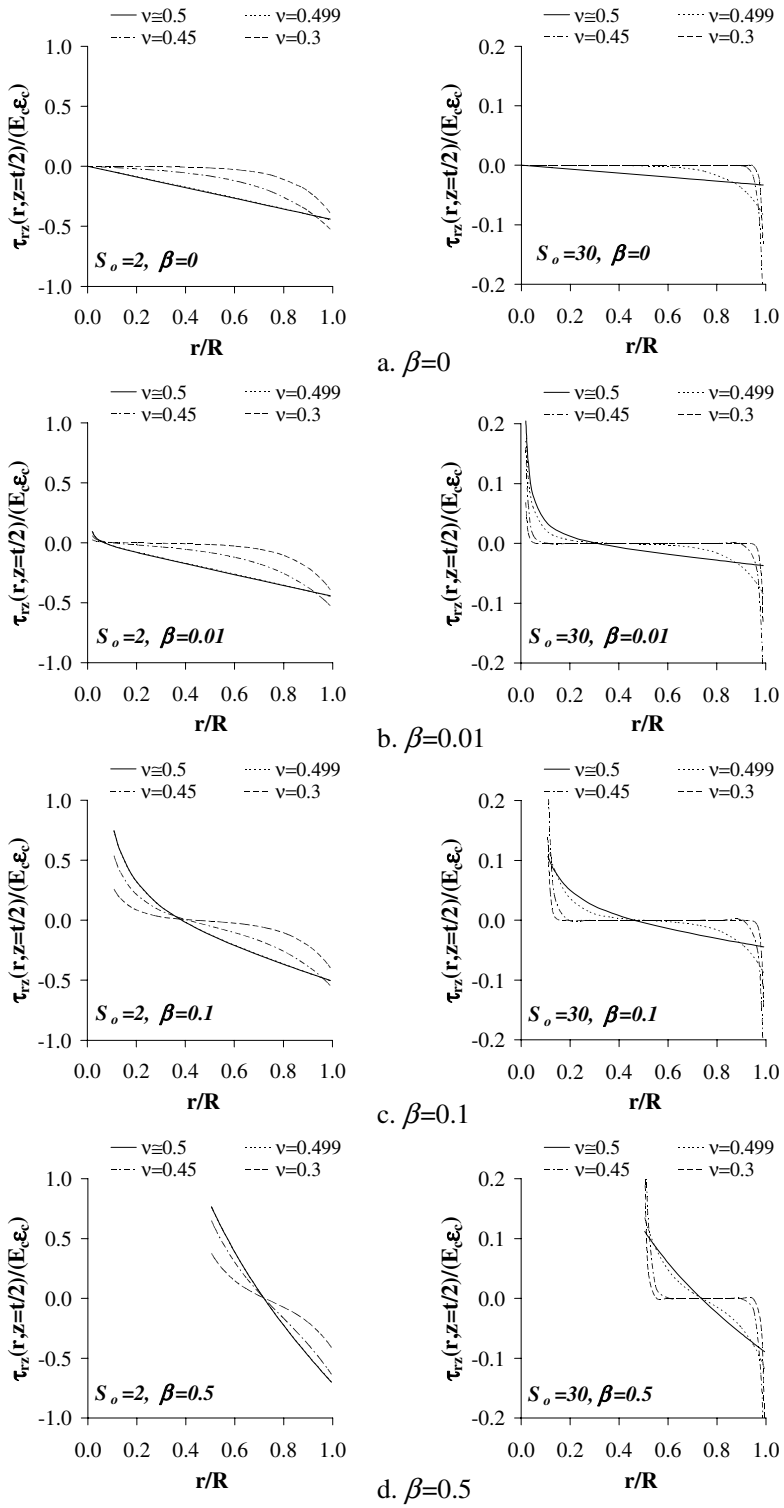

Fig. 9. Effect of radius ratio on shear stress distribution in radial direction in bonded annular layers with $S_0 = 2$ and $S_0 = 30$.

stress discontinuities are expected at the edges of the bonded faces, i.e., at $r = a$, $z = \pm t/2$ and at $r = R, z = \pm t/2$, because of different boundary conditions imposed on the bonded faces and lateral boundary (see Fig. 10):traction boundary conditions at the lateral force-free faces require that τ_{ri} $(i = r, \theta, z)$ be zero at $r = a$ and $r = R$, whereas no-slip condition at the bonded face of the layer together with constitutive equations require that $\tau_{rr} = \tau_{\theta\theta} = [\nu/(1-\nu)]\tau_{zz}$ at $z = \pm t/2$, which creates discontinuity in

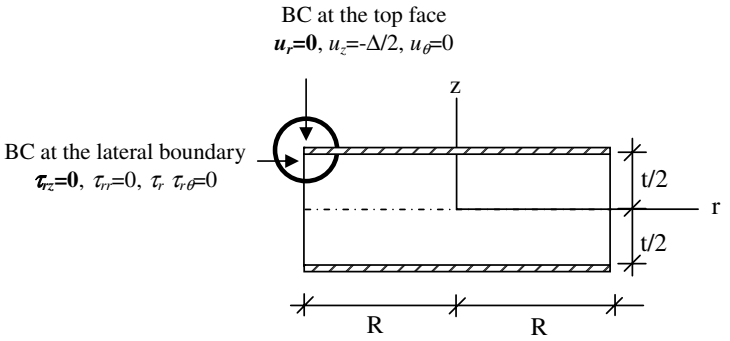

Fig. 10. Boundary conditions (BC's) at the edge of the bonded face of a solid circular disc.

radial stress τ_{rr}. On the other hand, the discontinuity of the shear stress τ_{rz} is due to that $\partial_z u_r \neq 0$ at the edge points of bonded faces (note the bulging of the lateral boundary). The above arguments explain why the shear stress distributions have non-zero values at the edges of the bonded faces. This point, i.e., the discontinuities occurring in τ_{rr} and τ_{rz} at the edges of bonded faces, was also pointed out and discussed by Papoulia and Kelly (1996). In the literature, it is further noted that "the effects of the edge singularity must be confined to extremely small regions in the neighborhood of the edges" (Gent et al., 1974) and that "the strength of the singularity decreases as the block gets thinner" (Ling et al., 1995). In view of Fig. 4, it may be noted also that FOT predictions in Fig. 9 for the shear stress τ_{rz} should be very close to the BEM results even near the edges of the bonded faces.

Now, a comment regarding the satisfaction of the lateral boundary conditions within the context of the approximate theory is in order. The approximate theory does *not require satisfying the lateral boundary conditions pointwise*; instead, it does it approximately in terms of the weighted averages of tractions over the thickness of the layer

$$\tau_{ri}^{n} = \frac{1}{2h}\int_{-h}^{+h} \tau_{ri}\phi_n \,\mathrm{d}z, \quad \text{where} \quad h = t/2, \quad i = (r,\theta,z), \quad n = (0-m), \quad m : \text{order of the theory} \tag{43}$$

to be specified along the boundary line of the horizontal section of the layer (see Eqs. (16) for these conditions for the compression of solid and annular discs). As m increases, the satisfaction of lateral boundary conditions by the approximate theory improves and becomes exact as $m \to \infty$. To display this numerically, we refer to Fig. 11 showing the distributions of shear stress τ_{rz} in radial direction at the sections z/t = (0.3, 0.4, 0.45, 0.49, 0.5) in an LSF solid disc with S = 2 and ν = 0.45. Comparison of ZOT and FOT results in that figure shows clearly the improvement in the satisfaction of the shear stress boundary condition on the lateral boundary as the order of the theory increases.

Fig. 12 shows radial stress τ_{rr} distributions at the center of the "ring" for S_0 = 2 and 30 for β = 0.1. To assess PM, its predictions (Constantinou et al., 1992) are also included in the graphs in discrete points. Similar to the solid case (Fig. 2), τ_{rr} distribution is uniform through the layer thickness for the HSF layer while it may be nonuniform in the LSF layer, in particular, when the material is strictly or nearly incompressible. Parallel with the earlier conclusion, PM fail to predict the behavior of bonded annular layers satisfactorily if S_0 or ν is small. As shown in Fig. 13, where, besides FOT predictions, the predictions of

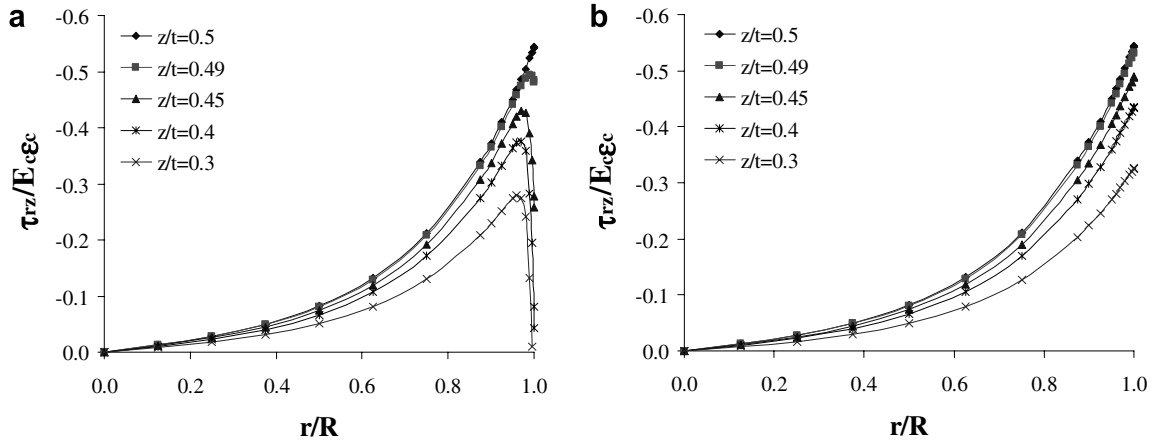

Fig. 11. (a) FOT and (b) ZOT predictions for shear stress distributions in radial direction in a bonded solid disc with S = 2 and ν = 0.45.

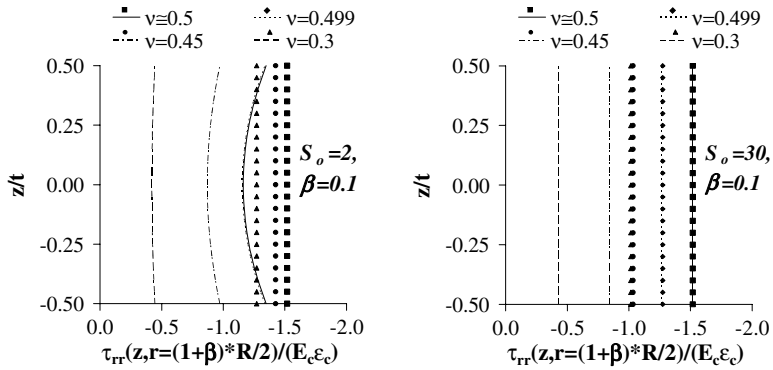

Fig. 12. Comparison of FOT (continuous lines) and PM (discrete points) predictions for radial stress distribution over the thickness of bonded annular ($\beta = 0.1$) discs for $S_0 = 2$ and $S_0 = 30$.

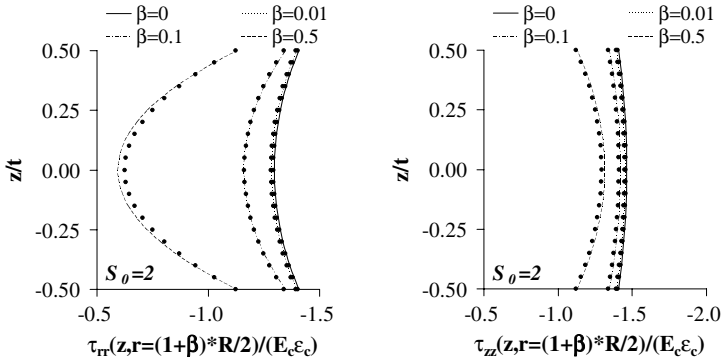

Fig. 13. Comparison of the predictions of FOT (continuous lines) and Ling (1996) (discrete points) for normal stress distributions over the thickness of bonded *incompressible* discs with $S_0 = 2$ for various radius ratios.

the expressions derived by Ling (1996) for incompressible materials are plotted for axial and radial stress distributions in vertical direction for an LSF layer ($S_0 = 2$) with different hole sizes, contrary to the PM solutions, the expressions derived by Ling (1996) can predict the nonlinearity in the distributions satisfactorily, for the reason stated previously in Section 4.1.

4.3. Maximum shear stresses and strains

From the graphs presented in Fig. 9, it may be seen that one of the major effects of the existence of a central hole in a bonded circular disc is its increasing the shear stress in the disc. The graphs in Fig. 14 show the effect of shape factor and Poisson's ratio on normalized maximum shear stress $(\tau_{rz})_{max}/E_c\varepsilon_c$ in a bonded C-disc, which occurs at ($r = R, z = \pm t/2$).

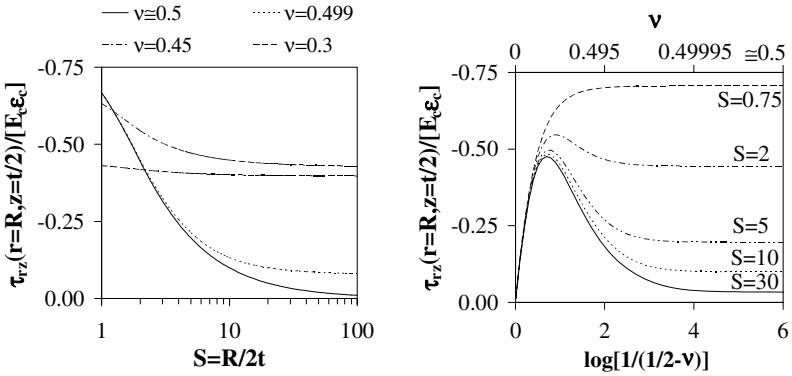

Fig. 14. Effect of shape factor and Poisson's ratio on maximum shear stress in a bonded solid disc.

As discussed in the previous section, there are two possible locations for $(\tau_{rz})_{max}$ in a bonded annular disc: either at the inner or at the outer edge of the bonded surfaces. However, it is rather difficult to predict exactly at which point $(\tau_{rz})_{max}$ occurs since this directly depends on β,S_0 and ν. The graphs presented in Fig. 15 plot the normalized shear stresses at the inner and outer edges as a function of S_0 for three different values of β. The study of Fig. 15 shows that both $\tau_{rz}(R,t/2)/E_c\varepsilon_c$ and $\tau_{rz}(\beta R,t/2)/E_c\varepsilon_c$ are influenced greatly by ν, i.e., by the material compressibility.

The comparison of the seconds of Fig. 15a and b shows that $\tau_{rz}(R,t/2)/E_c\varepsilon_c$ is not influenced from the existence of even a moderate-size hole in the center of the layer. On the other hand, the graphs in the firsts of Fig. 15a and b are considerably different, showing the strong effect of β on $\tau_{rz}(\beta R,t/2)/E_c\varepsilon_c$.

Considering that maximum shear strain (γ_{max}) is a special concern in the design of steel-laminated elastomeric bearings, it seems to be wise to investigate how it is affected by a hole in the center of a bonded annular disc. To this end, for design purposes, it is practical, as stated by Constantinou et al. (1992), to define a ratio named "magnification factor", to quantify the order of magnification in γ_{max} due to the existence of a central hole in a bonded annular disc. The graphs in Fig. 16 plot

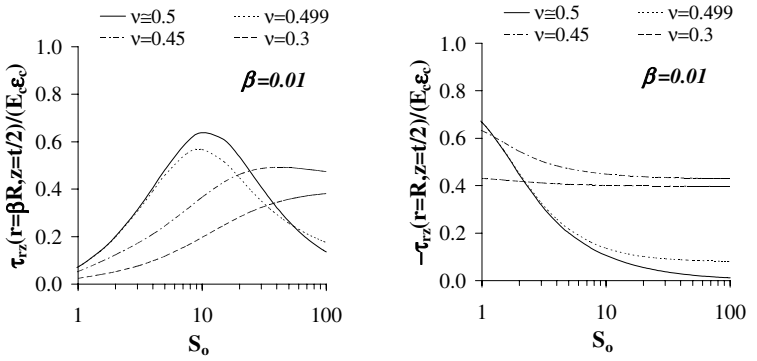

a. β=0.01

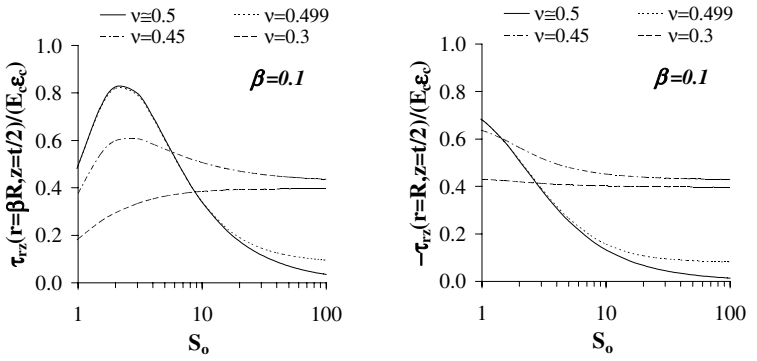

b. β=0.1

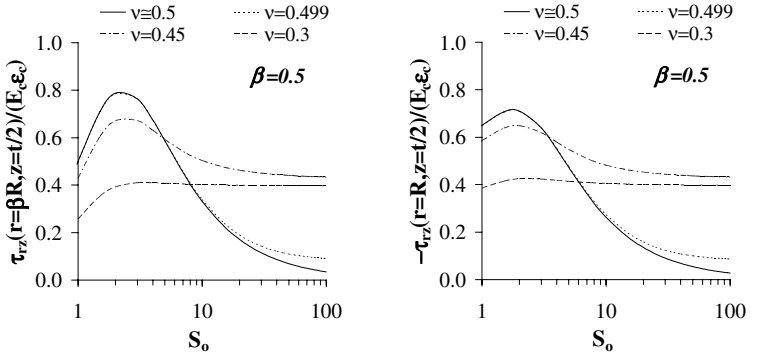

c. β=0.5

Fig. 15. Variation of shear stress at the inner (left hand side) and outer (right hand side) faces of a bonded annular layer with initial shape factor.

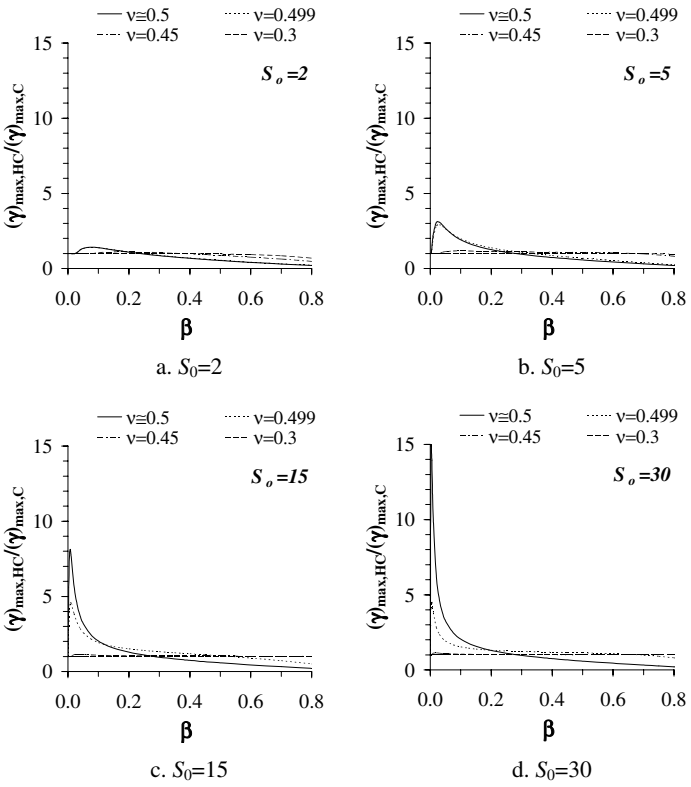

Fig. 16. Magnification of maximum shear strain due to the existence of a hole in the center of a bonded circular disc as a function of radius ratio.

this ratio, i.e., the ratio of the maximum shear strain in an HC-disc, denoted by $\gamma_{max,HC}$, to that in a C-disc with the same R/t value, denoted by $\gamma_{max,C}$, as a function of β for several values of S_0 and ν.

From Fig. 16, it may be observed that $\gamma_{max,HC}$ is not influenced significantly from β for compressible ($\nu \leqslant 0.45$) materials. On the other hand, the magnification factor can reach very large values for HSF layers with $\nu \cong 0.5$. For $S_0 = 30$, it is possible to have a magnification factor of as large as 15. Even the slight compressibility in the layer material can reduce this peak value considerably. For $S_0 = 30$, the ratio $\gamma_{max,HC}/\gamma_{max,C}$ has a peak value of 4.5 when $\nu = 0.499$, which is much smaller than the incompressible value of 15.

5. Conclusions

This paper presents analytical solutions to the problem of the uniform compression of bonded elastic layers in the shape of solid and annular circular discs. Closed-form expressions are derived for compression modulus and displacement/stress distributions by using the new formulation proposed by Pinarbasi et al. (2006) for linear analysis of bonded elastic layers. The use of first order theory (FOT) in the formulation leads to advanced solutions in view of that three of the commonly used assumptions in the literature are eliminated: (i) the incompressibility assumption, (ii) the "pressure" assumption and (iii) the assumption that plane sections remain plane after deformation. Advanced solutions derived using FOT are assessed by comparing their predictions with the numerical results obtained using boundary element method (BEM) and with the analytical solutions existent in the literature.

It should be noted that for the rigidly bonded disc problem analyzed in this study, there is no closed form, analytical exact elasticity solution, which requires pointwise satisfaction of governing equations at the points of solution domain and that of boundary conditions at the points of boundary surfaces. For that reason, the problem is handled by employing a refined approximate theory. This theory permits obtaining an approximate solution through the satisfaction of weighted averages over the thickness of the disc of governing equations in solution domain and of free traction boundary conditions on the lateral boundary. It is obvious that the satisfaction of free traction boundary conditions on the lateral boundary by the theory used in our analysis would be approximate and this approximation would improve as the order of theory increases (Fig. 11). It is to be noted that the lateral boundary of the disc does not include the edges of the top and bottom bonded faces of the disc, where the tractions may not vanish due to no-slip conditions imposed on these bonded faces. This is consistent with the results of boundary element method (Fig. 4) and with those reported by Papoulia and Kelly (1996).

It is obvious that elastomeric bearings may undergo large deformations during the motion induced by earthquakes, implying that their analysis should incorporate both the geometric and physical nonlinearities. However, since such analysis is very complicated and should be carried out after the linear behavior of elastomeric bearings is well understood, it is left to a future study; here, only the linear behavior of elastomeric bearings is considered.

Analytical solutions derived in the paper for the compression modulus and stress distributions are used to study the linear compressive behavior of rigidly bonded circular discs. Particular emphasis is given to the investigation of the effects of the existence of a central hole on compression modulus, stress distributions and maximum stresses/strains.

Main conclusions can be summarized as follows:

- Compressive behavior of a bonded annular disc with outer radius R, inner radius a and thickness t, is controlled by three main parameters: radius ratio of the hole $\beta = a/R$, Poisson's ratio of the elastic material ν and "initial shape factor" of the layer $S_0 = R/2t$.
- Compression modulus E_c of a bonded annular disc decreases with increasing β. This is mainly due to the fact that the presence of even a very small hole in the center of a bonded circular disc changes the axial stress distribution over the cross-section considerably especially if S_0 is large and ν is close to 0.5. Decrease in E_c with increasing β is *not* linear in general. For incompressible materials, E_c reduces abruptly near $\beta = 0$ especially if S_0 is large. For highly compressible materials (e.g., for $\nu = 0.3$), E_c of a bonded circular disc is almost independent of β.
- Normal stress distributions plotted over the layer thickness show that the "pressure" assumption is valid only for HSF layers of nearly/strictly incompressible materials. Stress distributions are nonuniform through the layer thickness for LSF layers especially if ν is close to 0.5.
- LSF layers reach their incompressible behavior at much smaller values of ν. For this reason, the compressive behavior of an LSF disc is not influenced significantly from the presence of slight compressibility in the material. On the other hand, the compressive behavior of HSF discs is affected from material compressibility substantially.
- Another important effect of the existence of a central hole in a bonded circular disc is its magnification of the maximum shear strain due to compression. "Magnification factor" can reach very large values for HSF layers especially if ν is close to 0.5. It is found that the existence of slight compressibility reduces the peak value of the magnification factor considerably.

Acknowledgement

This study is partially funded by the Turkish State Planning Organization Grant No. BAP-08-11-DPT2002K120510.

References

Chalhoub, M.S., Kelly, J.M., 1990. Effect of bulk compressibility on the stiffness of cylindrical base isolation bearings. International Journal of Solids and Structures 26, 743–760.
Constantinou, M.S., Kartoum, A., Kelly, J.M., 1992. Analysis of compression of hollow circular elastomeric bearings. Engineering Structures 14, 103–111.
Gent, A.N., Lindley, P.B., 1959. The compression of bonded rubber blocks. Proceedings of the Institution of Mechanical Engineers 173, 111–122.
Gent, A.N., Meinecke, E.A., 1970. Compression, bending and shear of bonded rubber blocks. Polymer Engineering and Science 10 (2), 48–53.
Gent, A.N., Henry, R.L., Roxbury, M.L., 1974. Interfacial stresses for bonded rubber blocks in compression and shear. Journal of Applied Mechanics 41, 855–859.
Holownia, B.P., 1972. Effect of Poisson's ratio on bonded rubber blocks. Journal of Strain Analysis 7, 236–242.
Kelly, J.M., 1997. Earthquake Resistant Design with Rubber. Springer-Verlag, London.
Lindley, P.B., 1968. Effect of Poisson's ratio on compression modulus. Journal of Strain Analysis 3, 142–145.
Lindley, P.B., 1979. Compression module for blocks of soft elastic material bonded to rigid end plates. Journal of Strain Analysis 14, 11–16.
Ling, Y.L., Engel, P.A., Brodsky, L., 1995. Compression of bonded annular rubber blocks. Journal of Engineering Mechanics 121 (6), 661–666.
Ling, Y., 1996. An approximate solution for the compression of a bonded thin annular disk. Journal of Applied Mechanics ASME 63 (3), 780–787.
Mengi, Y., 1980. A new approach for developing dynamic theories for structural elements. Part 1: Application to thermoelastic plates. International Journal of Solids and Structures 16, 1155–1168.
Moghe, S.R., Neff, H.F., 1971. Elastic deformations of constrained cylinders. Journal of Applied Mechanics ASME 38, 393–399.
Naeim, F., Kelly, J.M., 1999. Design of Seismic Isolated Structures. John Wiley & Sons Inc.
Ozkan, G., 1995. A Boundary Element Method for Axisymmetric Elastodynamic Analysis. Ph.D. Dissertation, Middle East Technical University, Ankara.
Papoulia, K.D., Kelly, J.M., 1996. Compression of bonded soft elastic material: variational solution. Journal of Engineering Mechanics ASCE 122, 1791–1805.
Pinarbasi, S., Akyuz, U., Mengi, Y., 2006. A new formulation for the analysis of elastic layers bonded to rigid surfaces. International Journal of Solids and Structures 43, 4271–4296.
Pinarbasi, S., Mengi, Y., 2008. Elastic layers bonded to flexible reinforcements. International Journal of Solids and Structures 45, 794–820.
Tsai, H.-C., Lee, C.C., 1998. Compressive stiffness of elastic layers bonded between rigid plates. International Journal of Solids and Structures 35, 3053–3069.